# Time-Resolved Spectroscopy and High Efficiency Light-driven Hydrogen Evolution of a Mo 3 S 4 -Containing Polyoxometalate-Based System

Yevheniia Smortsova, Clement Falaise, Anam Fatima, Minh-huong Ha-thi, Rachel Méallet-renault, Karine Steenkeste, Serge Al-bacha, Tesnim Chaib, Loïc Assaud, Marc Lepeltier, et al.

▶ **To cite this version:**

Yevheniia Smortsova, Clement Falaise, Anam Fatima, Minh-huong Ha-thi, Rachel Méallet-renault, et al.. Time-Resolved Spectroscopy and High Efficiency Light-driven Hydrogen Evolution of a Mo 3 S 4 -Containing Polyoxometalate-Based System. Chemistry - A European Journal, In press, ⟨10.1002/chem.202102693⟩. ⟨hal-03415475⟩

**HAL Id: hal-03415475**

**https://hal.science/hal-03415475v1**

Submitted on 4 Nov 2021

**HAL** is a multi-disciplinary open access archive for the deposit and dissemination of scientific research documents, whether they are published or not. The documents may come from teaching and research institutions in France or abroad, or from public or private research centers.

L'archive ouverte pluridisciplinaire **HAL**, est destinée au dépôt et à la diffusion de documents scientifiques de niveau recherche, publiés ou non, émanant des établissements d'enseignement et de recherche français ou étrangers, des laboratoires publics ou privés.

HAL Authorization

FULL PAPER

# Time-Resolved Spectroscopy and High Efficiency Light-driven Hydrogen Evolution of a {$Mo_3S_4$}-Containing Polyoxometalate-Based System

Yevheniia Smortsova,[a] Clément Falaise,[a] Anam Fatima,[b] Minh-Huong Ha-Thi,[b] Rachel Méallet-Renault,[b] Karine Steenkeste,[b] Serge Al-Bacha,[c] Tesnim Chaib,[a] Loïc Assaud,[c] Marc Lepeltier,[a] Mohamed Haouas,[a] Nathalie Leclerc,[a] Thomas Pino[b] and Emmanuel Cadot[a]

Dedication ((optional))

[a] Dr. Y. Smortsova, Dr. C. Falaise, Dr. M. Haouas, Dr. N. Leclerc and Pr. E. Cadot
ILV-CNRS UMR 8081, UVSQ, Université Paris-Saclay, 45, Avenue des Etats Unis, 78035 Versailles CEDEX, France
E-mail: clement.falaise@uvsq.fr
[b] A. Fatima, Dr. M.-H. Ha-Thi, Pr. R. Méallet-Renault, K. Steenkeste, Dr. T. Pino
ISMO-CNRS UMR 8214, Université Paris-Saclay
E-mail:
[c] Dr. S. Al-Bacha and Dr. L. Assaud
ICMMO-CNRS UMR 8182, Université Paris-Saclay, Rue du Doyen Georges Poitou, 91400 Orsay, France.

Supporting information for this article is given via a link at the end of the document

**Abstract:** Polyoxothiometalate ions are active hydrogen evolution reaction (HER) catalysts based on modular assembly build from electrophilic clusters {$MoS_x$} and vacant polyoxotungstates. Herein, the dumbbell-like anion $\{PW_{11}O_{39}\}_2(Mo_3S_4(H_2O)_3(OH))_2]^{8-}$ exhibits very high light-driven HER activity while the active cores {$Mo_3S_4$} do not contain any exposed disulphido ligands which were suspected at the origin of the HER activity. Moreover, in the catalyst architecture, the two central {$Mo_3S_4$} cores are sandwiched by two bulky $\{PW_{11}O_{39}\}^{7-}$ subunits that act as oxidant resistant protecting groups and behave as electron-collecting units. A detailed photophysical study was carried out confirming the reductive quenching mechanism of the photosensitizer $[Ir(bpy)_2(dtbbpy)]^+$ by the sacrificial donor triethanolammine (TEOA) and highlighting the very high rate constant for the electron transfer from the reduced photosensitizer to the Thio-POM catalyst. Such results provide new insight about HER activity of the Thio-POM catalysts.

## Introduction

Climate change is triggering many challenges and urgent needs in the renewable energy sources which are tackled intensively by the scientific community, including both the humanities and natural sciences. In light of the perspectives listed in the 2015 COP-21 Paris Agreement, solar energy with its huge potential became a horse to harness leading to an exponentially growing number of scientific publications. Harvesting and storage of the solar energy was confirmed to be a priority.[1] One of the possible solutions lays in the production of green solar fuel, i.e., via carbon-free catalytic processes. In context, solar-driven water splitting appears promising as sustainable energy conversion and storage process, crucial to convert the renewable sources from intermittent to viable energy in wind or solar power plants.[2] However, technical feasibility and technology readiness for green-hydrogen production and applications are still limited. Low efficiency and high cost of the most common approach used in solar to hydrogen energy-conversion systems, i.e., the photo-voltaic-electrolyzer interface, constitutes real drawbacks for industrial applications.[3] An alternative possibility consists to perform the "direct" solar-driven hydrogen production using efficient photocatalytic chemical systems. Implementation of such photosystems involves mastering interfaces between functional components including a photosensitizing unit and an active catalyst integrated into a single solar cell, which should be noble metal-free and highly efficient system.

In context, coordination chemistry concept allowed the design of a large variety of efficient catalysts for the Hydrogen Evolution Reaction (HER). The development of this class of Hydrogen Evolving Catalysts (HECs), using either bio-mimetic, or bio-inspired approach stems from mechanisms analysis of the functioning of hydrogenase enzymes. The binuclear active sites [Fe-Fe] or [Fe-Ni]-hydrogenase share both structural similarities corresponding to a bis-sulfido bridge that links the two metal centers. In addition, functioning of the [Fe-Fe]-type hydrogenase requires proximal protonation site and electron-shuttle unit to evolve hydrogen from a 2-electron and 2-proton process. This is achieved thank to a connected [4Fe-4S] cluster and a {N-H} group close to the [Fe-Fe] metal centers. It is clear that mechanistic studies have driven implementation of bio-mimetic systems paving the way toward rational molecular engineering of efficient bio-inspired photocatalytic systems. Besides, inorganically pure HECs such as amorphous molybdenum sulfides $MoS_x$ are broadly recognized as highly efficient HER catalysts for electro- and photo-driven HER based on earth-abundant elements.[4–7] Such $MoS_x$-type catalysts have been processed as heterogeneous solid-state catalysts within electro- or photo-electro catalysis but ill-defined $MoS_x$ deposited active phase makes intricate the HER

mechanism, wherein different active sites were proposed such as protonated disulfido and sulfido groups or $Mo^{V,IV}$-hydride. In the 70's-80's, fruitful molecular approaches have been deployed to model the active sites of the $MoS_2$-based catalysts used in the hydrodesulfurization (HDS) industrial processes. Actually, molecular thiomolybdate chemistry offers a large variety of clusters differing in their nuclearity, redox state, coordination pattern and bonding schemes useful to decipher the mechanisms and establish the structure-activity relationships. Besides, thiomolybdate clusters exhibit high HER efficiency, offering interesting opportunities to contribute to the development of advanced {Mo-S} catalysts, both in heterogeneous or homogeneous processes operating by electro- or photoelectro-activation. Among the discrete {Mo-S} species, both $[Mo_3S_{13}]^{2-}$ or $[Mo_2S_{12}]^{2-}$ clusters showed high activity in homogeneous visible-driven conditions thus demonstrating that such HEC-type catalysts could be promising candidates as catalytic components within the entire water-splitting solar cell.

On the other hand, polyoxometalates (POMs) constitute also an important class of electroactive compounds that found applications in many areas such as catalysis, energy storage with Li-ion and redox flow batteries or energy conversion processes. Due to their large diversity in terms of structure, composition and electronic properties, POMs chemistry provides an invaluable tool box for the fine design of electro- or photo- catalysts. For instance, polyoxotungstate ions constitute a library of electroactive ligands able to react with almost all the metallic cations. These rigid ligands act as clustering agent which, in many cases results in central metal clusters tightly nested between the surrounding polyoxotungstate groups. Among the plethoric examples, the tetraruthenium core $\{Ru_4O_4(OH)_4(H_2O)_4\}^{4+}$ stabilized by two $\gamma$-$[SiW_{10}O_{36}]^{8-}$ ligands behave as efficient water oxidation catalyst (WOC).[8],[9],[10] On the other hand, the tetranickel core $\{Ni_4\}^{8+}$ sandwiched by two $\alpha$-B-$[PW_9O_{34}]^{9-}$ trivacant anion or the $\{Ni_{14}\}$ grafted onto $\{SiW_9O_{34}\}^{10-}$ exhibit both high photocatalytic efficiency for hydrogen evolution reaction.[11],[12] Using such an approach, the active thiomolybdic core $\{Mo_3S_4\}^{4+}$ has been grafted on the hexavacant crown-shaped anion $[H_7P_8W_{48}O_{184}]^{33-}$.[13] The resulting mixed $Mo_3S_4$-containing POM was shown to be a very efficient electrocatalyst for HER, functioning either in homogeneous or in heterogeneous conditions, as deposited co-catalyst on silicon photocathode.[14] Such a strategy was demonstrated as a general efficient approach to synthesize polymodular thio-POM species that exhibit various combinations, stoichiometries and structures.[15] In context, we report on the combination of the $\{Mo_3S_4\}$ core with the monovacant anion $\alpha$-A-$[PW_{11}O_{39}]^{7-}$ resulting of a similar structure scheme of that previously reported for the $[\{(SiW_{11}O_{39})Mo_3S_4(H_2O)_3(\mu\text{-}OH)\}_2]^{10-}$ cluster.[16] This thio-POM, formulated as $[\{(PW_{11}O_{39})Mo_3S_4(H_2O)_3(\mu\text{-}OH)\}_2]^{8-}$ reveals to behave as efficient HER catalyst through visible light-driven process. In addition, comparison with other reported efficient POM-based systems or thiomolybdates allow identifying this class of compounds as very promising candidates as HER catalysts.

Furthermore, along with the demonstration of the pertinence of the thio-POM strategy for the design of efficient homogeneous HER photocatalysts, the mechanism of the solar-driven hydrogen evolution was addressed through a thorough photophysical investigation of the successive processes succeeding the photon absorption by the photosensitizing unit. This study helped to rationalize the observations made in photocatalytic experiments involving the novel thio-POM catalyst. The full understanding of the HER-productive pathway is crucial for further improvements of this new class of photocatalytic systems.

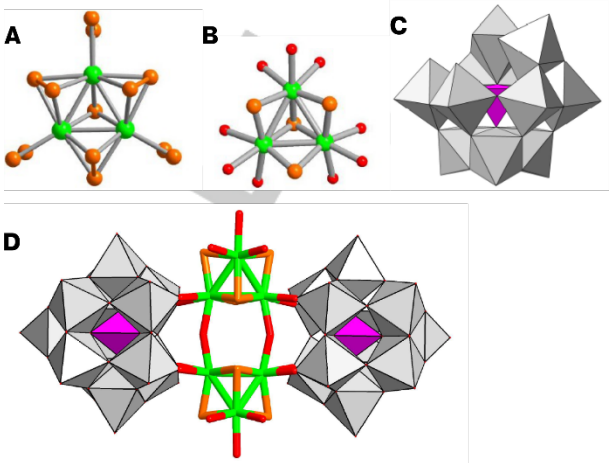


**Figure 1** Structural representations of: (A) $[Mo_3S_{13}]^{2-}$, (B) $[Mo_3S_4(H_2O)_9]^{4+}$, (C) $[PW_{11}O_{39}]^{7-}$ and (D) $[\{(PW_{11}O_{39})Mo_3S_4(H_2O)_3(\mu\text{-}OH)\}_2]^{8-}$ (Chalco-POM). Structural representation of the thio-POM resulting from the combination between $[Mo_3S_4(H_2O)_9]^{4+}$ and $\alpha$-A-$[PW_{11}O_{39}]^{7-}$ ions was derived from the reported structure of $[\{(SiW_{11}O_{39})Mo_3S_4(H_2O)_3(\mu\text{-}OH)\}_2]^{10-}$ cluster species (see ref 16).

## Results and Discussion

**Synthesis.** The protocol of synthesis was derived from that previously reported by Müller et al. wherein the monovacant $\alpha$-A-$[SiW_{11}O_{39}]^{8-}$ ion was substituted for the $\alpha$-A-$[PW_{11}O_{39}]^{7-}$ precursor, which reacts with the $\{Mo_3S_4(H_2O)_9\}^{4+}$ aquo cluster in nearly stoichiometric condition. The resulting thioanion was isolated as mixed cesium-sodium salt from pH 2 aqueous solution. Characterizations including elemental analysis, EDS, infrared, $^{31}P$ NMR and UV-vis were in fair agreement with the structural arrangement resulting from the single-crystal X-ray diffraction analysis of the $[\{(SiW_{11}O_{39})Mo_3S_4(H_2O)_3(\mu\text{-}OH)\}_2]^{10-}$ (see Figure 1). Such a molecular arrangement consists of two central $\{Mo_3S_4(H_2O)_3\}$ cores linked together by two hydroxo briges. Then, the resulting central cationic unit $\{Mo_6S_8(OH)_2(H_2O)_6\}^{6+}$ is sandwiched by two peripheral monovacant subunits $\alpha$-A-$[PW_{11}O_{39}]^{7-}$ subunits, giving the dumbbell-like arrangement. Synthesis and characterization of complex **1** were detailed in Supporting Information (SI).

### Hydrogen Evolution Reaction

**Electrocalysis.** As preliminary experiments, investigations of the electrocatalytic HER activity of the dumbbell-like arrangement $PW_{11}$-$Mo_3S_4$ has been conducted in homogenous conditions in 0.5 mol.$L^{-1}$ $H_2SO_4$ aqueous solution (pH ≈ 0.3) (see Figure 2). In such conditions, no significant HER process was observed in the presence of the polyoxotungstate ion $\alpha$-A-$[PW_{11}O_{39}]^{7-}$ until about -0.3 V *vs* RHE. However, it should be worth noting that in such acidic conditions, the $\alpha$-A-$[PW_{11}O_{39}]^{7-}$ monovacant anion is no

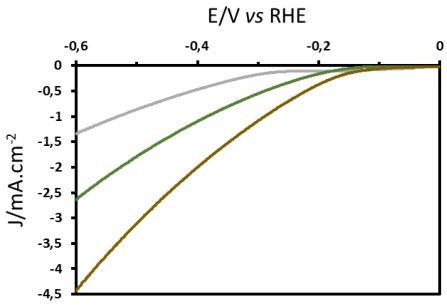


**Figure 2.** Polarization curves of 5 × $10^{-4}$ mol $L^{-1}$ thio-POM $PW_{11}$-$Mo_3S_4$ (brown), $\{Mo_3S_4\}$ (green), and $\{PW_{11}\}$ (grey) recorded on glassy carbon showing the highest efficiency of the hybrid $\{Mo_3S_4\}$-containing POM catalyst in 0.5 mol $L^{-1}$ aqueous sulfate solution pH = 1 (scan rate = 50 mV $s^{-1}$).

longer stable and converts slowly into the saturated Keggin anion $\alpha$-$[PW_{12}O_{40}]^{3-}$. In contrast, in the presence of the $\{Mo_3S_4\}$-based anion $[\{(PW_{11}O_{39})Mo_3S_4(H_2O)_3(\mu\text{-}OH)\}_2]^{8-}$, the CV exhibits a noticeable increase of the cathodic current that occurs from about -0.15 V *vs* RHE. Similar behavior was also observed with the POM-free $\{Mo_3S_4\}$ cluster although the cathodic current was significantly lower than those observed with the mixed $PW_{11}$-$Mo_3S_4$ catalyst. Actually, such qualitative experiments appear fully consistent with our previous reported results and demonstrate that the synergistic electrocatalytic HER effect arising from the covalent linking between polyoxotungstate ions and $\{Mo_3S_4\}$ cluster can be generalizable to various POM-$Mo_3S_4$ combinations.

**Photocatalysis.** Determination of the HER light-driven photocatalytic activity of the thio-POM compound as tetrabutylamonium salt was carried out using similar conditions that those reported by Hill et al. with a tetra-nickel polyoxotungstate ion.[11] The photochemical system is made up of three complementary components with $[Ir(ppy)_2(dtbbpy)]^+$ (noted [Ir], with ppy = 2-phenylpyridine and dtbbpy = 4,4'-di-*tert*-butyl-2,2'-bipyridine) as photosensitizing unit, triethanolamine (TEOA) as sacrificial electron/proton donor and $PW_{11}$-$Mo_3S_4$ as catalyst. Then, measure of the hydrogen evolution has been carried out from photochemical system with composition corresponding to [TEOA] = 0.3 mol.$L^{-1}$, [Ir] = 0.2 mmol.$L^{-1}$ and [catalyst] = 40 μmol.$L^{-1}$ in a dimethylformamide (DMF)/$CH_3CN$ solution (10 mL, 3:1v). Using blue-light-emitting diodes ($\lambda$ = 450 nm, ~ 2.4 mW) at 25°C for the photolysis, a quasi-linear increase of the hydrogen production with time is observed. For benchmarking these photochemical performances, we compared catalytic efficiency of the thio-POM system with other reported catalytic systems such as Ni-containing POM anions which correspond to one of the best achievements in the field. Using same photochemical conditions, visible-light-driven HER of $[Ni_4(H_2O)_2(PW_9O_{34})_2]^{10-}$ and $[(SiW_9O_{34})Ni_{14}(AleH)_5(Ale)_2(H_2O)_{11}(OH)_7]^{12-}$ anions as tetrabutylamonium (noted TBA•$Ni_4P_2$) salt and bis(triphenylphosphoranylidene)ammonium (noted PPN•$Ni_{14}Si$) salt, respectively, have been investigated. Results obtained with these Ni-containing POMs are included in Figure 3 for comparison with those of the thio-POM compound as TBA salt (noted TBA•$Mo_3S_4$-PW). Control experiments have revealed that the three components of the photochemical system are

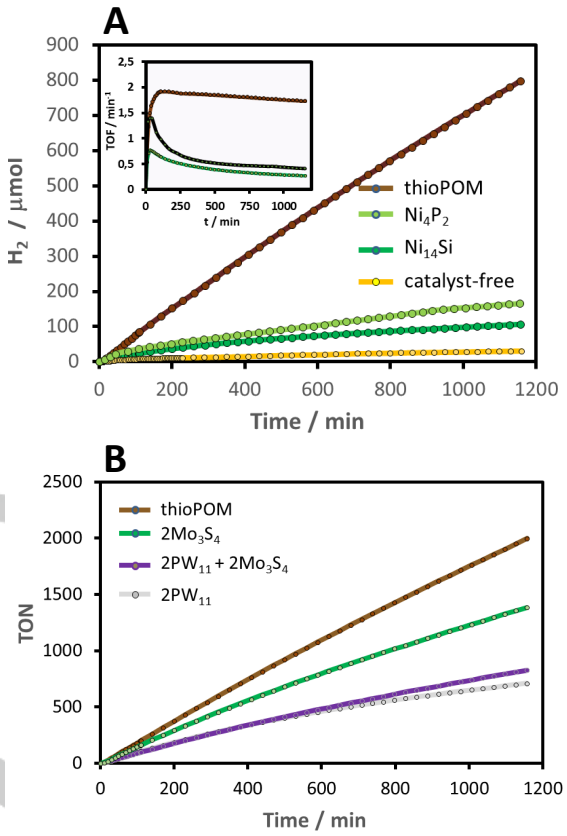


**Figure 3.** A) Photocatalitic activity of the thio-POM anion compared to that of the nickel-containing POMs and to catalyst-free system; insert: Variation of the Turn-Over-Frequency (TOF) with time showing the fair photocatalytic stability of the thio-POM system compared to the other two Ni-containing POMs. Conditions: thio-POM, 34 μM (brown curve), $Ni_{14}Si$, 36 μM (dark green curve), $Ni_4P_2$, 37 μM (ligth-green curve), LED light (2.4 mW, 450 nm), $[Ir(ppy)_2(dtbbpy)]^+$ (0.2 mM), TEOA (0.3 M), 2 mL $CH_3CN$/DMF (1/3) deaerated with Ar. B) Turn-Over-Number of the various components of the thio-POM systems. The TON was calculated taking into account the dimeric nature of the thio-POM. Conditions: [thio-POM] = 40 μM, [$2Mo_3S_4$] = 39.5 μM, [$2PW_{11}$] = 40 μM and [$2Mo_3S_4$-$2PW_{11}$] = 39 μM; TEOA, 0.325 mM, [Ir] = 0,2 mM.

complementary for the HER process. The thio-POM catalyst was not able to produce hydrogen in the absence of either the [Ir] photosensitizing or the sacrificial electron donor TEOA. However, it should be worth mentioning that association of [Ir] complex with TEOA leads to a weak HER activity (see Figure 3A). In short, after 15 h, the thio-POM system exhibits a TON of ~1700 while in similar conditions, both Ni-containing POM anions give significantly lower turnover such as ~300 and ~400 for $Ni_{14}Si$ and $Ni_4P_2$, respectively. These contrasted results are illustrated nicely by the variation of the TOF with time given for each compound (see Figure 3A, insert). Furthermore, the photocatalytic HER activity has been also measured independently for the constituting units of the thio-POM catalyst, i.e., $\{Mo_3S_4\}$ as a PPN salt of nitrilotriacetate (NTA) complex and $[PW_{11}O_{39}]^{7-}$ as TBA salt. As shown in Figure 3B,

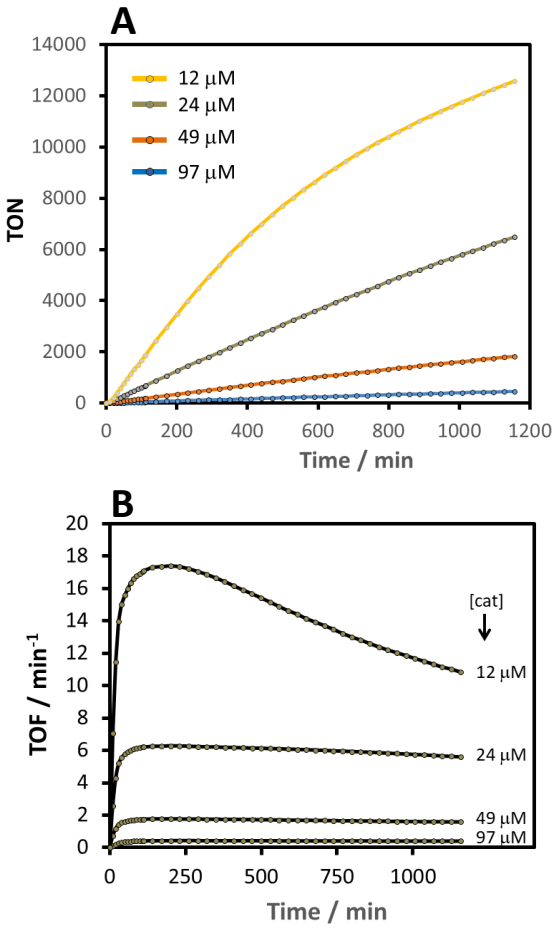


**Figure 4.** A) Variation of TON with time as a function of the catalyst concentration. Conditions: [thio-POM] = 10-100 µM, [TEOA] = 0.325 M), [Ir] = 235 µM, 10 mL $CH_3CN$/DMF (1/3) deaerated with Ar. B) Highlighting the strong dependence of Turn-Over-Frequency (TOF) on the concentration in thio-POM.

the covalent linkage between the central core $\{[Mo_3S_4(OH_2)_3(OH)]_2\}^{6+}$ and the two POM subunits α-A-$[PW_{11}O_{39}]^{7-}$ is featured by higher TON (TON = 1700 after 15 h), while in similar conditions, the $[Mo_3S_4(HNTA)_3]^{2-}$ coordination complex exhibits about 25% smaller TON = 1150 (see Figure 3b). In addition, it should be worth noting that the monovacant anion $[PW_{11}O_{39}]^{7-}$ is also able to produce hydrogen (TON = 620 after 15 h). At last, catalytic activity of a mixture containing equimolar $[Mo_3S_4(HNTA)_2]^{2-}$ and α-A-$[PW_{11}O_{39}]^{7-}$ was measured showing that the presence of thiocluster $\{Mo_3S_4\}$ does not give any benefit to the HER activity which remains similar to that observed for the α-A-$[PW_{11}O_{39}]^{7-}$ anion. Such a behavior could be explained tentatively by ion-pairing competition of both anionic units, i.e., α-A-$[PW_{11}O_{39}]^{7-}$ and $[Mo_3S_4(HNTA)_3]^{2-}$ with the cationic photosensitizing component. Such a competition process should favor mostly electrostatic associations involving the highest negatively charged species $[PW_{11}O_{39}]^{7-}$ with the monocationic photosensitizer $[Ir(ppy)_2(dtbbpy)]^+$ (noted [Ir]). Then, in such conditions, photo-induced electron transfer should occur mostly from [Ir] toward the $[PW_{11}O_{39}]^{7-}$ ion, where the latter becomes the main catalytically active component, thus quenching the activity of the $[Mo_3S_4(HNTA)_2]^{2-}$ unit.

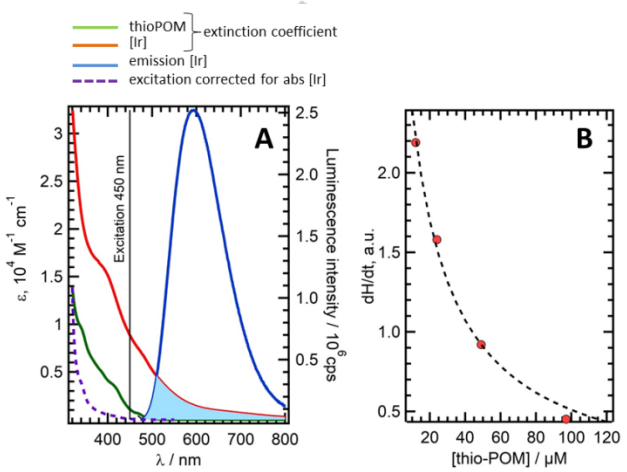


**Figure 5.** A) Extinction coefficient of [Ir] (dark-green) and thio-POM (red) in $CH_3CN$/DMF (1/3). Emission (blue) and excitation (pink) spectra of [Ir] in $CH_3CN$/DMF (1/3) deaerated solution. The overlap between the thio-POM absorption and [Ir] luminescence is highlighted by the light-blue colored area. B) Variation of $V_{app}$ versus the concentration of thio-POM, consistent with the absorption of thio-POM as predominant detrimental effect upon the rate of $H_2$ evolution. Red circles = experimental data and black dotted line = calculated data using the semi-quantitative model expressed by equation (8) (see Suplementary Information for further details).

Furthermore, the HER activity, the rate of the $H_2$ evolution and then the TOF depend also on the concentration of the thio-POM catalyst. Nevertheless, these kinetic parameters exhibit surprisingly a significant increase as the concentration in thio-POM catalyst decreases, while the initial concentrations in [Ir] and TEOA were kept constant ([TEOA] = 0.325 M and [Ir] = 235 µM) (see Figure 4 and Figure SI 1, in SI). Such dependence is remarkable because as the thio-POM concentration has been decreased from 100 to 10 µM, the TOF increases dramatically within a magnitude of 45 times from 0.4 to about 18 $min^{-1}$ (see Figure 4). As shown in Figure 4A, for a 12 µM concentration in catalyst, the TON reaches 2500 after 2.5 h, thus showing the very high HER efficiency of this thio-POM anion. Similar experiments were carried out on the Ni-containing POM catalysts, such as $Ni_4P_2$ or $Ni_{14}Si$, but an opposite effect was observed, corresponding to an increase of the rate of $H_2$ evolution as the concentration of catalyst increases.[11],[12] Analysis of the optical properties of the absorbing species gives some insight to further understand such behavior.

**Steady-state absorption and emission**

Steady-state absorption, emission and excitation spectra of the photosensitizer and the absorption spectrum of the photocatalyst are shown in Figure 5A. The absorption of [Ir] at 450 nm is assigned to the $S_0 \rightarrow S_1$ metal-to-ligand charge transfer (MLCT) transitions ($Ir_d$-π*),[17] while the luminescence originates from the triplet state $[Ir]^T$. The maximum emission is observed at 590 nm. The luminescence excitation spectrum matches the absorption one above 450 nm. As the excitation spectrum does not show higher-energy bands, excitation to higher excited states should result in ultrafast non-radiative relaxation which should not interfere with chemical reactions. In addition, the excitation emission matrix shows that the emission and excitation spectra are not dependent on the excitation and emission wavelength,

respectively (see Figure SI 2, in SI). Hence, only one emissive species of [Ir] is present in the solution.

Besides, the extinction coefficient of thio-POM in the visible range is about 9 times larger than that of [Ir] photosensitizer (see Figure 5A). The absorptions of the photocatalyst in the visible region arise from the {$Mo_3S_4$} chromophore. These absorptions correspond to $Mo^{IV}$-centered d-d transitions and E→Mo LMCT (with E = S, O)[18,19] which are characteristic of {$Mo_3S_4$} covalently linked to polyoxotungstate units.[20] Moreover, a study of a similar compound with α-A-$[SiW_{11}O_{39}]^{8-}$ as lacunary Keggin subunits reported that both {$Mo_3S_4$} units are almost electronically uncoupled.[16] At working concentrations, the portion of light absorbed by the [Ir] at 450 nm is about 47% while in the presence of thio-POM, the attenuation of light in the most concentrated solution equals 98.8% for 2 cm optical path of the reactor. In such conditions, the portion of light absorbed by the photosensitizer falls down to 1.6%. These observations allow to explain qualitatively the sharp decrease of the efficiency of the photocatalytic production of $H_2$ with the increase of the concentration of the thio-POM (see Figure 5B). Moreover, the thio-POM absorbs in the wavelength range of the luminescence of [Ir]. The large overlap of these spectra is highlighted in Figure 5A (blue area) and indicates the possibility of energy transfer from the excited state of [Ir] to the catalyst. A similar iridium complex associated to an iron-containing catalyst as an acceptor evidenced such process, as reported by Lochbrunner et al.[21] Furthermore, the rate of $H_2$ evolution is also dependent upon the concentration of the photosensitizer [Ir] (see details SI, Figure SI 1, meaning that the determining step of the process involves both the phosensitizer and the catalyst. This could correspond to electron transfer from reduced iridium complex (noted [Ir°]) to the catalyst according to equation (1). Such an elemental step leads to the rate law given in equation (2) where $k$, $C_{[Ir^\circ]}$ and $C_{cat}$,

$$[Ir^\circ] + \text{thio-POM} \rightarrow [Ir] + \text{thio-POM}^{red} \quad (1)$$

$$V = \frac{dH_2}{dt} = kC_{[Ir^\circ]} \cdot C_{cat} \quad (2)$$

correspond to the kinetic constant of the determining step, the concentration of reduced iridium complex [Ir°] and the concentration of thio-POM, respectively. The concentration of [Ir°] depends on i) the initial concentration in [Ir], which was kept constant in experiments shown in Figure 4, and ii) the concentration in thio-POM because this species absorbs strongly visible light that cancels the formation of active [Ir°], and also because thio-POM species is able to quench significantly the formation of excited iridium species [Ir]* through energy transfer process with consequence to decrease the formation of [Ir°]. The absorption of visible-light by the thio-POM species could be roughly expressed from the Beer-Lambert law shown in equation (3), where ε and L are the average molar absorption coefficient of the solution (dominated by catalyst's value) and L the optical path related to geometry of the cell. In such conditions, the effective concentration in [Ir°] species is attenuated by the variable coefficient $k_{ii}$ given by equation (4).

$$I_t = I_0 10^{-\varepsilon L C_{cat}} \quad (3)$$

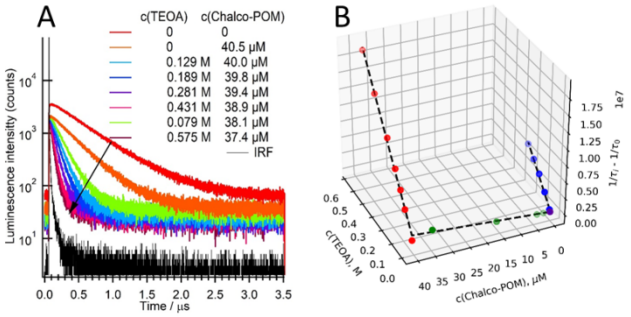


**Figure 6.** A) Luminescence intensity decays of [Ir] with different concentrations of TEOA and thio-POM in $CH_3CN$/DMF (1/3) solution. Instrument response function (IRF) is shown in black. The concentration of [Ir] was 0.2 mM. Excitation and emission wavelengths were 469 and 569 nm, respectively. B) Stern-Volmer analysis of the experiments where the iridium complex was mixed with i) TEOA - blue, ii) – thio-POM -green and iii) both TEOA and thio-POM - red. The fit is shown as black broken lines.

$$A_{ii} = k_{ii}\frac{I_0}{\varepsilon \cdot C_{cat}}[1 - 10^{-\varepsilon L C_{cat}}] \quad (4)$$

Furthermore, the quenching process can be described by the Stern-Volmer equation (5) that expresses the intensity of luminescence as a function of the concentration in quencher, i.e., the thio-POM catalyst. In equations (5) and (6), $K_{SV}$ corresponds to the Stern-Volmer parameter such as $K_{SV} = k_{q_i} \times \tau_0$ where $k_{q_i}$ and $\tau_0$ are the Stern-Volmer quenching constant and the life time of Ir excited triplet-state (noted $[Ir]^T$) in the absence of quencher, respectively. Both attenuating coefficients

$$\frac{I_0}{I} = 1 + K_{SV} \cdot c_{cat} \quad (5)$$

$$A_{iii} = k_{iii}\frac{I_0}{1 + K_{SV} \cdot c_{cat}} \quad (6)$$

i.e., $A_{ii}$ and $A_{iii}$ from equations (4) and (6), respectively, can be used to express the concentration of [Ir°] in equation (7) that gives at last equation (8). The full details of the analysis are given in supplementary information.

$$C_{[Ir^\circ]} = C_{[Ir]} \times \varphi \times A_{ii} \times A_{iii} \quad (7)$$

$$V = \frac{dH_2}{dt} = \frac{a}{1 + bC_{cat}}[1 - 10^{-cC_{cat}}] \quad (8)$$

Then, equation (8) contains three parameters, noted *a*, *b* and *c* which have been adjusted to reproduce satisfactorily the experimental data. As shown in Figure 5B, this semi-quantitative model gives comprehensive basis to explain the variation of the HER activity in respect to the concentration of the thio-POM catalyst. At last, the dependence of the electron donor TEOA on the HER rate has been also examined showing a quasi-first-order kinetic regime for concentration in TEOA smaller than 0.3 mol.$L^{-1}$ and a nearly non-dependent for higher concentration meaning that in such a concentration range, the determining elementary step is no longer the formation of [Ir°] from TEOA, but rather the electron transfer process from the photosensitizer to the catalyst expressed in equation (1). In addition, it should be mentioned that during long time experiment, the solution undergoes a color change from orange-yellow to green-blue, consistent with the reduction of the polyxotungstate subunits in the stationary state. Further investigations were carried out to pinpoint the electron-transfer process by means of time-resolved spectroscopy.

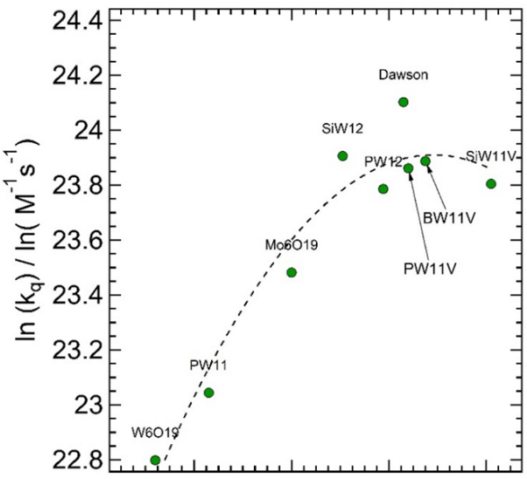


**Figure 7.** Marcus plot for quenching of [Ir] by a family of polyoxometalates: the Linqvist-type $[W_6O_{19}]^{2-}$ and $[Mo_6O_{19}]^{2-}$, the monovacant Keggin $[PW_{11}O_{39}]^{7-}$, the Dawson $[P_2W_{18}O_{62}]^{7-}$, the Keggin α-$[SiW_{12}O_{40}]^{4-}$ and α-$[PW_{12}O_{40}]^{3-}$ , and the mixed metal W-V Keggin derivatives $[PW_{11}VO_{40}]^{4-}$, $[SiW_{11}VO_{40}]^{5-}$, and $[BW_{11}VO_{40}]^{6-}$ anions.

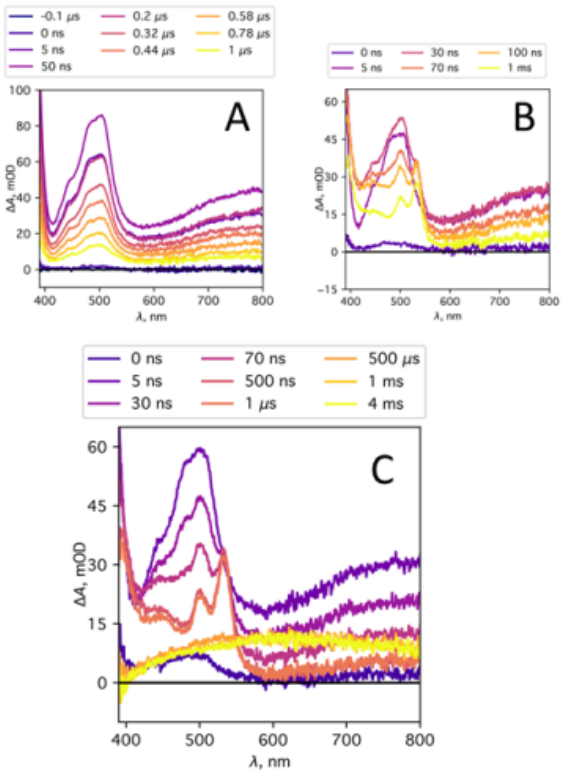


**Figure 8.** Nanosecond transient absorption spectra in $CH_3CN$/DMF (1/3) of A) 0.19 mM [Ir], B) 0.20 mM [Ir] / 325 mM TEOA, C) 0.20 mM [Ir] / 323 mM TEOA / 0.040 mM thio-POM. Spectra in A) are corrected for luminescence, in B) for luminescence and baseline, and C) for fluo and baseline. Spectra in C) are fixed delay spectra.

**Time-resolved spectroscopy**

**Time-resolved emission.** The interaction with the excited state of the photosensitizer is always manifested by changes in excited state lifetimes. For emissive entities, these changes can be monitored by the measurement of the luminescence intensity decays (LIDs). The LIDs of [Ir] solutions in DMF/$CH_3CN$ (3:1v) with different concentrations of TEOA and thio-POM were acquired for three different sets of experiments, where [Ir] complex was mixed successively with (i) TEOA, (ii) thio-POM and (iii) both TEOA and thio-POM. The LIDs for the set (iii) are presented in Figure 6A and show a gradual decrease of the excited state lifetime of [Ir] upon addition of TEOA or thio-POM. This decrease reflects exchange interactions in both systems $[Ir]^T$/TEOA and $[Ir]^T$/thio-POM. The optimized parameters of the monoexponential fit of the data which are given in Table SI 1, in SI. Stern-Volmer analysis of the experiments (i), (ii) and (iii) (see Figure 6B) gave quenching constants of $2.9 \cdot 10^7$ $M^{-1}$ $s^{-1}$ (i) and $3.0 \cdot 10^7$ $M^{-1}$ $s^{-1}$ (iii) for TEOA and $5.1 \cdot 10^{10}$ $M^{-1}$ $s^{-1}$ (ii) and $4.3 \cdot 10^{10}$ $M^{-1}$ $s^{-1}$ (iii) for thio-POM. The obtained constants are very close in the experiments where two quenchers are present apart or together in the solution. Therefore, the interactions $[Ir]^T$/TEOA and $[Ir]^T$/thio-POM can be separated and do not influence each other. Luminescence quenching studies are commonly employed to determine whether a reductive or oxidative quenching cycle is operative in a particular reaction.[22] From the emission results, one can conclude that the HER follows both oxidative and reductive pathways. The nature of the interaction that causes the quenching may be further revealed by electrochemical measurements of the redox potentials of [Ir], TEOA and thio-POM in DMF/$CH_3CN$ (3:1v). These show that both reductive and oxidative quenching pathways are possible. Electron transfer between an iridium organic complex and a polyoxometalate was observed in dyads by femtosecond transient absorption.[24] Based on these results, one can anticipate that the electron transfer may be efficient in bimolecular dynamic quenching. According to Marcus theory, in case of electron transfer between a molecule in an excited state and the quencher, the dependence of the logarithm of the quenching constant on the driving force of the electron transfer has a characteristic bell shape. This dependence is shown in Figure 7. In order to obtain the desired quenching products, one need the successor complex to escape the solvation cage.[23] Transient absorption experiments allowed exploring such process.

**Transient absorption spectroscopy**

**Photosensitizer.** Femtosecond transient absorption (TA) spectra of [Ir] in DMF/$CH_3CN$ using 400 nm excitation are shown in Figure SI 5. Solvent Raman signals are visible until 0.25 ps. After 0.25 ps, the spectra are dominated by the excited state absorption band of [Ir]. Between 0.3 ps and 1 ps, the bands at 500 nm and in NIR, starting from 600 nm, increase. From 1 ps, and to 14 ps, the band around 450 nm decreases, and the two bands at 500 nm and in NIR, starting from 600 nm, continue to grow. After 14 ps the spectra do not change anymore. Global analysis of these data gave the 2 time constants after correction of the solvent Raman signal: 1.37 ps and one much longer than the measured time window. Using nanosecond transient absorption, the kinetics of

$[Ir]^T$ can be modelled by monoexponential function, convoluted with a Gaussian pulse of 3 ns width. The lifetime of the excited state is about 490 ns. In Figure 8A, one can see a broad absorption band at 500 nm and a less intense absorption band, stretching to the near-infrared. The shapes of the 1 ns delay femtosecond TA and of the nanosecond TA spectra perfectly match (see Figure SI17, in SI).

**Photosensitizer and electron donor.** Nanosecond transient spectra of [Ir] and TEOA solution shows $[Ir]^T$ signature at early times (0 and 5 ns) (see Figure 8B). The appearance of a new spectroscopic feature is observed as a double peak at 530 and 500 nm. This feature is attributed to reduced [Ir] ($[Ir]^0$), as observed in literature. [25,26] The experiments with a reversible electron donor 1,4-diazabicyclo[2.2.2]octane (DABCO) show the same signature assigned to the photosensitizer reduced state (Figure SI 7, in SI). Multi-exponential global fit of [Ir]/TEOA kinetics gave the time constants of 64 ns and 8.9 µs, as well as an infinite time component (see decay associated spectra and chosen kinetics in Figures SI 8 and SI 9, SI). The 64 ns component corresponds to the formation of reduced [Ir], while the one at 8.9 µs is clearly the recombination of reduced [Ir] and oxidized TEOA. The infinite time component is the residual reduced [Ir], as the oxidized TEOA is not stable and takes part in the following reactions.[27,28] The $y_0$ spectrum corresponds to the inverted infinite time component and is the same as the baseline, acquired at -100 ns.

**Photosensitizer and thio-POM.** The quenching of [Ir] by thio-POM does not show any new spectroscopic signature in nanosecond transient spectra (see the decay associated spectra - DAS of [Ir]/thio-POM system on Figure SI 6). Therefore, the hypotheses about the electron or energy transfer cannot be confirmed, although they remain plausible. Indeed, the lifetime of the excited state of thio-POM resulted from energy transfer process is very short and can not be observed in nanosecond TA measurements and a fast recombination within the solvent cage may not lead to any efficient formation of charge separated state.[24]

**Photosensitizer, electron donor and thio-POM.** Nanosecond transient spectra of [Ir], TEOA and thio-POM is shown in Figure 8C. At 0 ns and 5 ns, the signature of $[Ir]^T$ is observed. Then, the signature of reduced [Ir] is visible up to 1 µs. A new broad and featureless signature appears later and lasts longer than the time window of the measurement (4 ms). Once formed, no changes are observed in this band. The global fit of these data gives the time constants of 57 ns, 1.41 µs and 100 µs. The resulting DAS are shown in Figure SI 14, in SI. The first time constant, 57 ns, clearly corresponds to the reductive quenching of [Ir] by TEOA. 1.41 µs and 100 µs time components have the DAS characteristic for the decay of reduced [Ir]. The infinite time component DAS reproduced the shape of the spectrum of the photoproduct, formed in a light-induced reaction (see Figure 8C, 500 µs, 1 ms and 4 ms spectra). Similarly to the system with TEOA, the $y_0$ spectrum corresponds to the inverted infinite time component and is the same as the baseline acquired at -100 ns. Moreover, the difference steady-state spectrum of the same solution (after / before illumination, Figure SI 16, in SI) follows perfectly the shape of 1 ms and 4 ms TA spectra.

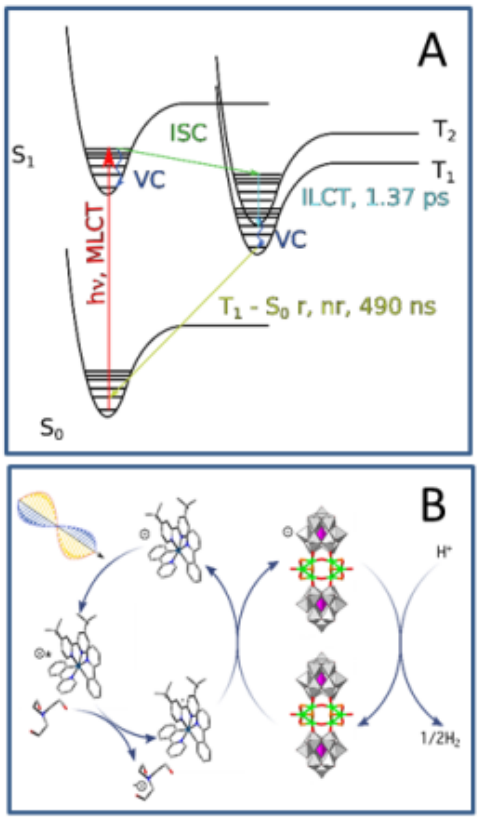


**Figure 9.** A) Proposed hypothesis of the excited state dynamics of [Ir] in $CH_3CN$/DMF (1/3), based on femto- and nano-second TA experiments and literature data. B) Proposed mechanism of the sunlight-driven HER in [Ir]/TEOA/thio-POM system.

In order to clarify the nature of the photoproduct, nanosecond TA experiments with the two components $[PW_{11}O_{39}]^{7-}$ and $[Mo_3S_4(Hnta)_3]^{2-}$ were conducted. Transient spectra at indicated delay times for the system [Ir]/TEOA/{$PW_{11}O_{39}$} are presented in Figure SI 18, in SI. The spectra at 0 ns and 5 ns after the excitation are characteristic for $[Ir]^T$. In consistency with the previously presented systems, $[Ir]^T$ is quenched by TEOA (time constant of 72 ns, see Figure SI 18, in SI) with appearance of reduced [Ir], visible in the spectra from 30 ns to 1 ms. At 500 µs, a broad spectral feature appears and lasts until 4 ms without relaxation (infinite time component, Figure SI 18, in SI). This feature is assigned to the photoproduct, which must have a very similar nature to the photoproduct formed in the photosystem [Ir]/TEOA/thio-POM. The reduced [Ir] disappears with a time constant of 280 µs. The nanosecond transient spectrum at -100 ns corresponds to the baseline $y_0$.

The nanosecond transient spectra of the system [Ir]/TEOA/$PPN_2Mo_3S_4Hnta_3$ at indicated delays are presented in Figure SI 19, in SI. Similarly to the previous measurements, the spectra at 0 ns and 5 ns after the excitation correspond to the $[Ir]^T$ that is quenched by TEOA with a time constant of 62 ns (Figure

SI 19, in SI). The relaxation of the reduced [Ir] is multi-exponential and longer than the time window of the measurement, but could be well described with time constants of 9.3 µs, 390 µs and an infinite time signal. A new band at 435 nm can be seen on the spectra starting from 500 µs and up to 4 ms. The decrease in the band intensity observed when the spectrum at 4 ms is compared to the one at 500 µs, would be rather due to the relaxation of $[Ir]^0$, as $[Ir]^0$ difference spectrum partly overlaps this region, and not to the decrease in the concentration of the photoproduct. The nature of this photoproduct is obviously different than the nature of that formed in previously discussed systems [Ir]/TEOA/thio-POM and [Ir]/TEOA/{$PW_{11}$}.

**Mechanism of the HER process**

The thio-POM strategy[15] has been used to design a new type of photocatalyst for homogeneous HER. The new catalyst was produced by combination of a molecular cluster core {$Mo_3S_4$} and a monovacant {$PW_{11}$} POM as a proton/electron collecting module and outperforms the catalysts for homogeneous solar-driven hydrogen evolution, reported so far in literature. An important synergistic effect between the molecular cluster {$Mo_3S_4$} and {$PW_{11}$} moieties is evidenced by the photocatalytic experiments (see Figure 3B).

Then, photophysical investigations were performed in order to provide more understanding and insights of the successive events taking place after light absorption by the photosensitizer. On the basis of the femtosecond TA measurements on [Ir] and literature data,[17,29,30] a hypothesis about the excited state dynamics of [Ir] complex was elaborated. After absorption of a photon, the two different singlet MLCT states resulted of positive electronic density changes on phenylpyridyl (ppy) and 4,4'-di-tert-butyl-2,2'-bipyridyl (dtb-bpy) ligands are formed and they undergo an ultrafast intersystem crossing (ISC) to form triplet MLCT excited states of the ppy and dtb-bpy ligands, respectively. The former triplet state undergoes an interligand charge transfer from ppy to dtbbpy and forms a triplet state with a positive electronic density change on dtbbpy ligand in 1.37 ps. After, this triplet state is stable for about 490 ns (lifetime) in DMF/$CH_3CN$ solution and then is available for the photochemical reactions. This hypothesis is illustrated in Figure 9A.

In addition, $[Ir]^T$ state is quenched in presence of TEOA or thio-POM. While the quenching by TEOA was shown to be of reductive nature with formation of $[Ir]^0$ in accordance to previous reports,[25,26,31] the interaction $[Ir]^T$/thio-POM can only be indirectly attributed to energy and electron transfers. Indeed, while the absorption and emission spectra of thio-POM and $[Ir]^T$ overlap (see Figure 5) and the Marcus plot has its characteristic shape (see Figure 7), neither the excited state of thio-POM nor the reduced thio-POM were observed in nanosecond transient spectra of [Ir]/thio-POM system. An extremely short lifetime of the thio-POM excited state and fast electron recombination of the donor-acceptor pair are possible mechanisms to prevent direct observations of $[Ir]^T$ interaction with thio-POM. Importantly, the 'no-deal' quenching of $[Ir]^T$ by thio-POM frustrates the oxidative pathway of solar-driven HER in the system [Ir]/TEOA/thio-POM.

In [Ir]/TEOA/thio-POM nanosecond TA experiments, the $[Ir]^0$ signal decays and a flat and broad signal of a photoproduct appears with a similar kinetic (Figure SI 15, in SI). The spectrum of the photoproduct is visible also in the steady-state spectrum after the illumination (Figure SI 16, in SI). The nature of this photoproduct can be ascribed with a large probability to the reduced catalyst. Indeed, reduced polyoxometalates absorption usually features broad bands above 600 nm that expand toward the near infra-red.[32–34] Although the shape of this absorption depends on the coordination of the vacant POM moieties, the similarity of the 4 ms nano-TA differential spectra in [Ir]/TEOA/thio-POM and [Ir]/TEOA/{$PW_{11}$} systems points that the coordination of {$PW_{11}$} to {$Mo_3S_4$} unit does not result in a strong electronic coupling. Overall observations enable us to put forward a mechanism of the hydrogen evolution. Non-productive quenching of $[Ir]^T$ by thio-POM along with the decay of $[Ir]^0$ signal and concomitant rise of broad signal of reduced thio-POM in nanosecond transient spectra in Figure 8C are strong evidences in favor of the reductive HER pathway for this system as shown in Figure 9B. The reductive pathway can be considered as beneficial to the stability of the photosensitizer,[35] as in the oxidized state there is a possibility of the nucleophilic attack of the ligands.[36] However, the decomposition of the iridium heteroleptic complexes in reduced state was also reported, suggesting the importance of reducing the time needed to relay the electron by the photosensitizer.[37]

According to the proposed mechanism given in Figure 9B, the large quenching constant of thio-POM is detrimental for the HER and it is critical to maintain the concentration of the sacrificial donor much higher than that of the thio-POM in order to get the maximum yield. In fact, high concentration of the catalyst interferes the hydrogen evolution, as shown in Figure 5B. The ratio between products of rate constants of quenching and the concentration of the quencher TEOA/thio-POM $k_{q,TEOA}\cdot[TEOA]/k_{q,thioPOM}\cdot[thioPOM]$ is ≈ 16 for the solution with 12 µM thio-POM and is only ≈ 2 for 97 µM thio-POM solution, thus giving a half of excited photosensitizer being quenched through non-productive pathway. Moreover, the synergy effect of combining {$Mo_3S_4$} and {$PW_{11}$} is also partly boosted by the increase of the concentration of the quenching entities.

In view of the much higher concentration of the catalyst with respect to the concentration of $[Ir]^0$ in the system after the photoexcitation, one can assume the pseudo-first order rate law of the electron transfer from $[Ir]^0$ to the catalyst:[38] $k = 1/\tau\cdot[thioPOM]$. The rates of this process were calculated to be 25, 3.2, and 4.5 x $10^7$ $M^{-1}s^{-1}$ for thio-POM, $PPN_2Mo_3S_4Hnta_3$ and $TBA_7PW_{11}O_{39}$, respectively. Much higher rate constant of charge transfer to the catalyst can be the key of its high efficiency as photocatalyst. The use of the thio-POM catalyst can raise the 'electronic burden' from the photosensitizer earlier and thus increase its stability that ensure its availability for the following sunlight-driven HER cycles.

Several literature reports claim that the terminal disulfide bridges are essential for the HER using molybdenum sulfide materials as catalysts.[39,40] thio-POM does not share such a structural pattern

and exhibits high performance and stability in solar-driven HER. This observation hints that the part of the mechanism of the HER that starts from the reduction of thio-POM by $[Ir]^0$ may be partly responsible for the activity of molecular $\{MoS_x\}$ models. Further investigations are needed in order to elucidate this point. For example, multiple electron reduction of thio-POM can be tracked, using EPR, Raman and IR spectroscopy techniques[41,42] or steady-state UV-Vis absorption in absence of oxidized species[43].

## Conclusion

For the first time, homogeneous catalysis of solar-driven HER using a thio-POM $\{Mo_3S_4\}\{PW_{11}\}$ assembly was reported. The efficiency of this novel thio-polyoxometalate outperforms the reported nickel-based catalyst and proves the synergy effect of molybdenum sulfide cluster and polyoxometalate proton/electron storage and stabilizing unit. However, photo-physical investigations evidenced the reductive quenching mechanism of the process, showing that high rate constant of the electron transfer between the reduced photosensitizer and the thio-POM is at the origin of the high performance of this novel catalyst. These results pave the way toward the fine implementation of such novel molecular thio-POM type catalysts.

## Experimental Section

Experimental Details.

## Acknowledgements

The authors gratefully acknowledge LabEx CHARMMMAT grants (ANR-11-LBX-0039, **NUMBER**), ANR (Agence Nationale de la Recherche) CHALCO-CAT program (CHALCO-CAT ANR-15-CE06-0002-01), the Centre National de la Recherche Scientifique (CNRS), the Ministère de l'Education Nationale de l'Enseignement Supérieur et de la Recherche (MENESR), the University of Versailles Saint Quentin (UVSQ) and the University Paris-Saclay for their financial support. The authors acknowledge LASIRE UMR 8516 laboratory for the use of the femtosecond transient absorption.

**Keywords:** polyoxometalate • thiomolybdate • HER • photocalysis • spectroscopy

[1] M. A. K. Lodhi, *International Journal of Hydrogen Energy* **1989**, *14*, 379–411.
[2] B. Widera, *Thermal Science and Engineering Progress* **2020**, *16*, 100460.
[3] S. E. Hosseini, M. A. Wahid, *Renewable and Sustainable Energy Reviews* **2016**, *57*, 850–866.
[4] M. Kokko, F. Bayerköhler, J. Erben, R. Zengerle, Ph. Kurz, S. Kerzenmacher, *Applied Energy* **2017**, *190*, 1221–1233.
[5] M.-L. Grutza, A. Rajagopal, C. Streb, P. Kurz, *Sustainable Energy Fuels* **2018**, *2*, 1893–1904.
[6] P. D. Tran, T. V. Tran, M. Orio, S. Torelli, Q. D. Truong, K. Nayuki, Y. Sasaki, S. Y. Chiam, R. Yi, I. Honma, J. Barber, V. Artero, *Nature Materials* **2016**, *15*, 640–646.
[7] J. Kibsgaard, T. F. Jaramillo, F. Besenbacher, *Nature Chemistry* **2014**, *6*, 248–253.
[8] Y. V. Geletii, C. Besson, Y. Hou, Q. Yin, D. G. Musaev, D. Quiñonero, R. Cao, K. I. Hardcastle, A. Proust, P. Kögerler, C. L. Hill, *J. Am. Chem. Soc.* **2009**, *131*, 17360–17370.
[9] F. M. Toma, A. Sartorel, M. Iurlo, M. Carraro, P. Parisse, C. Maccato, S. Rapino, B. R. Gonzalez, H. Amenitsch, T. Da Ros, L. Casalis, A. Goldoni, M. Marcaccio, G. Scorrano, G. Scoles, F. Paolucci, M. Prato, M. Bonchio, *Nature Chem* **2010**, *2*, 826–831.
[10] M. Bonchio, Z. Syrgiannis, M. Burian, N. Marino, E. Pizzolato, K. Dirian, F. Rigodanza, G. A. Volpato, G. La Ganga, N. Demitri, S. Berardi, H. Amenitsch, D. M. Guldi, S. Caramori, C. A. Bignozzi, A. Sartorel, M. Prato, *Nature Chemistry* **2019**, *11*, 146–153.
[11] H. Lv, W. Guo, K. Wu, Z. Chen, J. Bacsa, D. G. Musaev, Y. V. Geletii, S. M. Lauinger, T. Lian, C. L. Hill, *Journal of the American Chemical Society* **2014**, *136*, 14015–14018.
[12] G. Paille, A. Boulmier, A. Bensaid, M.-H. Ha-Thi, T.-T. Tran, T. Pino, J. Marrot, E. Rivière, C. H. Hendon, O. Oms, M. Gomez-Mingot, M. Fontecave, C. Mellot-Draznieks, A. Dolbecq, P. Mialane, *Chem. Commun.* **2019**, *55*, 4166–4169.
[13] R. Contant, A. Teze, *Inorg. Chem.* **1985**, *24*, 4610–4614.
[14] J. Tourneur, B. Fabre, G. Loget, A. Vacher, C. Mériadec, S. Ababou-Girard, F. Gouttefangeas, L. Joanny, E. Cadot, M. Haouas, N. Leclerc-Laronze, C. Falaise, E. Guillon, *J. Am. Chem. Soc.* **2019**, *141*, 11954–11962.
[15] E. Cadot, M. N. Sokolov, V. P. Fedin, C. Simonnet-Jégat, S. Floquet, F. Sécheresse, *Chem. Soc. Rev.* **2012**, *41*, 7335–7353.
[16] A. Müller, V. P. Fedin, C. Kuhlmann, H. Bögge, B. Hauptfleisch, V. P. Fedin, H.-D. Fenske, G. Baum, *Chem. Commun.* **1999**, 1189–1190.
[17] S. Tschierlei, A. Neubauer, N. Rockstroh, M. Karnahl, P. Schwarzbach, H. Junge, M. Beller, S. Lochbrunner, *Phys. Chem. Chem. Phys.* **2016**, *18*, 10682–10687.
[18] D. Fu, B. Fabre, G. Loget, C. Mériadec, S. Ababou-Girard, E. Cadot, N. Leclerc-Laronze, J. Marrot, Q. de Ponfilly, *ACS Omega* **2018**, *3*, 13837–13849.
[19] S. Duval, M.-A. Pilette, J. Marrot, C. Simonnet-Jégat, M. Sokolov, E. Cadot, *Chemistry – A European Journal* **2008**, *14*, 3457–3466.
[20] J. Tourneur, B. Fabre, G. Loget, A. Vacher, C. Mériadec, S. Ababou-Girard, F. Gouttefangeas, L. Joanny, E. Cadot, M. Haouas, N. Leclerc-Laronze, C. Falaise, E. Guillon, *J. Am. Chem. Soc.* **2019**, *141*, 11954–11962.
[21] A. Neubauer, G. Grell, A. Friedrich, S. I. Bokarev, P. Schwarzbach, F. Gärtner, A.-E. Surkus, H. Junge, M. Beller, O. Kühn, S. Lochbrunner, *J. Phys. Chem. Lett.* **2014**, *5*, 1355–1360.
[22] C. K. Prier, D. A. Rankic, D. W. C. MacMillan, *Chem. Rev.* **2013**, *113*, 5322–5363.
[23] J. W. Tucker, C. R. J. Stephenson, *J. Org. Chem.* **2012**, *77*, 1617–1622.
[24] B. Matt, X. Xiang, A. L. Kaledin, N. Han, J. Moussa, H. Amouri, S. Alves, C. L. Hill, T. Lian, D. G. Musaev, G. Izzet, A. Proust, *Chem. Sci.* **2013**, *4*, 1737–1745.
[25] H. Lv, W. Guo, K. Wu, Z. Chen, J. Bacsa, D. G. Musaev, Y. V. Geletii, S. M. Lauinger, T. Lian, C. L. Hill, *Journal of the American Chemical Society* **2014**, *136*, 14015–14018.
[26] G. Paille, A. Boulmier, A. Bensaid, M.-H. Ha-Thi, T.-T. Tran, T. Pino, J. Marrot, E. Rivière, C. H. Hendon, O. Oms, M. Gomez-Mingot, M. Fontecave, C. Mellot-Draznieks, A. Dolbecq, P. Mialane, *Chem. Commun.* **2019**, *55*, 4166–4169.
[27] B. Probst, A. Rodenberg, M. Guttentag, P. Hamm, R. Alberto, *Inorganic Chemistry* **2010**, *49*, 6453–6460.
[28] Y. Pellegrin, F. Odobel, *Comptes Rendus Chimie* **2017**, *20*, 283–295.
[29] C. W. Stark, W. J. Schreier, J. Lucon, E. Edwards, T. Douglas, B. Kohler, *J. Phys. Chem. A* **2015**, *119*, 4813–4824.
[30] G. J. Hedley, A. Ruseckas, I. D. W. Samuel, *J. Phys. Chem. A* **2009**, *113*, 2–4.
[31] S. I. Bokarev, D. Hollmann, A. Pazidis, A. Neubauer, J. Radnik, O. Kühn, S. Lochbrunner, H. Junge, M. Beller, A. Brückner, *Phys. Chem. Chem. Phys.* **2014**, *16*, 4789–4796.
[32] E. Papaconstantinou, *Chem. Soc. Rev.* **1989**, *18*, 1–31.
[33] T. Minato, T. Matsumoto, S. Ogo, *RSC Adv.* **2019**, *9*, 19518–19522.
[34] C. Lee, C. R. Keenan, D. L. Sedlak, *Environ Sci Technol* **2008**, *42*, 4921–4926.
[35] M. Natali, F. Puntoriero, C. Chiorboli, G. La Ganga, A. Sartorel, M. Bonchio, S. Campagna, F. Scandola, *J. Phys. Chem. C* **2015**, *119*, 2371–2379.
[36] P. K. Ghosh, B. S. Brunschwig, M. Chou, C. Creutz, N. Sutin, *J. Am. Chem. Soc.* **1984**, *106*, 4772–4783.
[37] L. L. Tinker, N. D. McDaniel, P. N. Curtin, C. K. Smith, M. J. Ireland, S. Bernhard, *Chemistry – A European Journal* **2007**, *13*, 8726–8732.
[38] Z.-J. Li, F. Zhan, H. Xiao, X. Zhang, Q.-Y. Kong, X.-B. Fan, W.-Q. Liu, M.-Y. Huang, C. Huang, Y.-J. Gao, X.-B. Li, Q.-Y. Meng, K. Feng, B. Chen, C.-H. Tung, H.-F. Zhao, Y. Tao, L.-Z. Wu, *J. Phys. Chem. Lett.* **2016**, *7*, 5253–5258.

[39] M. Dave, A. Rajagopal, M. Damm-Ruttensperger, B. Schwarz, F. Nägele, L. Daccache, D. Fantauzzi, T. Jacob, C. Streb, *Sustainable Energy Fuels* **2018**, *2*, 1020–1026.
[40] A. Rajagopal, F. Venter, T. Jacob, L. Petermann, S. Rau, S. Tschierlei, C. Streb, *Sustainable Energy Fuels* **2019**, *3*, 92–95.
[41] D. Hollmann, F. Gärtner, R. Ludwig, E. Barsch, H. Junge, M. Blug, S. Hoch, M. Beller, A. Brückner, *Angewandte Chemie International Edition* **2011**, *50*, 10246–10250.
[42] S. Fischer, O. S. Bokareva, E. Barsch, S. I. Bokarev, O. Kühn, R. Ludwig, *ChemCatChem* **2016**, *8*, 404–411.
[43] B. Matt, J. Fize, J. Moussa, H. Amouri, A. Pereira, V. Artero, G. Izzet, A. Proust, *Energy Environ. Sci.* **2013**, *6*, 1504–1508.

WILEY-VCH

## Entry for the Table of Contents

Insert graphic for Table of Contents here. ((Please ensure your graphic is in **one** of following formats))

((max. width: 5.5 cm; max. height: 5.0 cm))

**Please delete this box prior to submission**

((max. width: 11.5 cm; max. height: 2.5 cm))

**Please delete this box prior to submission**

Insert text for Table of Contents here. ((The Table of Contents text should give readers a short preview of the main theme of the research and results included in the paper to attract their attention into reading the paper in full. The Table of Contents text **should be different from the abstract** and should be no more than 450 characters including spaces.))

Institute and/or researcher Twitter usernames: ((optional))

WILEY-VCH